Editors' Suggestion

Andreev Reflection in Scanning Tunneling Spectroscopy of Unconventional Superconductors

P. O. Sukhachov,[1,*] Felix von Oppen,[2] and L. I. Glazman[1]
[1]Department of Physics, Yale University, New Haven, Connecticut 06520, USA
[2]Dahlem Center for Complex Quantum Systems and Fachbereich Physik, Freie Universität Berlin, 14195 Berlin, Germany

(Received 13 September 2022; accepted 2 May 2023; published 25 May 2023)

We evaluate the differential conductance measured in an STM setting at arbitrary electron transmission between STM tip and a 2D superconductor with arbitrary gap structure. Our analytical scattering theory accounts for Andreev reflections, which become prominent at larger transmissions. We show that this provides complementary information about the superconducting gap structure beyond the tunneling density of states, strongly facilitating the ability to extract the gap symmetry and its relation to the underlying crystalline lattice. We use the developed theory to discuss recent experimental results on superconductivity in twisted bilayer graphene.

DOI: 10.1103/PhysRevLett.130.216002

Introduction.—The structure of the superconducting order parameter is a defining property of unconventional superconductors [1]. The latter range from high-T_c superconductors such as Ba-doped $LaCuO_3$ [2] and $BiSrCaCu_2O_x$ [3] to novel moiré materials such as twisted bilayer (TBG) and trilayer (TTG) graphene [4–13] or twisted double-layer copper oxides [14–18]. In high-T_c superconductors, the large value of the gap allowed one to study its momentum dependence via angle-resolved photoemission spectroscopy [19]. The gap symmetry of high-T_c materials was also confirmed by quasiparticle interference [20,21]. The much smaller gaps of superconducting TBG and TTG along with the small sample dimensions complicate the use of angle-resolved photoemission spectroscopy, while the large-period moiré pattern impedes the quasiparticle interference method. That brings scanning tunneling spectroscopy (STS) to the fore.

Recent works on TBG and TTG [12,13] reveal a V-shaped profile of the differential conductance as a function of bias in the traditional STS regime of weak tunneling (tip relatively far from the sample). This was interpreted as evidence for nodal (d-wave) superconductivity. The observation of an enhanced low-bias conductance in the strong-tunneling regime (tip forming a point contact with TBG) was viewed [12] as evidence of Andreev reflection, further confirming the unconventional nature of superconductivity in hole-doped TBG.

This experiment prompted us to develop a theory of point-contact tunneling into superconductors with arbitrary gap structures and for arbitrary transmission coefficients of the contact [22]. As tip-sample tunneling does not conserve momentum, it is difficult to reconstruct the gap structure solely from the differential conductance in the weak-tunneling regime. In this regime, the differential conductance yields the energy dependence of the tunneling density of states, which carries some information on the momentum dependence of the absolute value of the gap. Our theory provides access to considerably more extensive information, including the gap symmetry, by synthesizing data taken in the weak- and strong-tunneling regimes. The additional information enters through the phase sensitivity of Andreev reflections, which dominate STS data in the strong-tunneling limit [26].

Scattering matrix formalism for STM tip.—We view the contact between tip and two-dimensional (2D) system as a single-mode quantum point contact opening into a (super) conducting sheet of material. For a pointlike tip and assuming time-reversal symmetry (TRS) of the normal state so that $s(\varepsilon) = s^T(\varepsilon)$, the contact can be described by the two-channel scattering matrix

$$s(\varepsilon) = \begin{pmatrix} s_0'(\varepsilon) & t(\varepsilon) \\ t(\varepsilon) & s_0(\varepsilon) \end{pmatrix}. \tag{1}$$

The amplitude $s_0'(\varepsilon)$ describes reflection between incoming and outgoing channels in the tip, and the transmission amplitude $t(\varepsilon)$ controls the differential conductance of the contact in the normal state, $G_n(V) = G_Q|t(eV)|^2$ [27]. Here, $G_Q = e^2/(\pi\hbar)$ is the conductance quantum.

A pointlike tip couples to a single channel of the 2D system, so that scattering between in- and outgoing waves in the 2D system is described by the S-matrix element $s_0(\varepsilon)$. For a uniform system, $s_0(\varepsilon)$ describes scattering in the zero angular momentum channel: an arbitrary incoming wave ψ^{in} in the substrate is scattered into the outgoing wave $\psi^{\text{out}} = [(\hat{I} - \hat{P}) + s_0(\varepsilon)\hat{P}]\psi^{\text{in}}$, with $\hat{P}$ projecting onto zero angular momentum. A reflectionless junction between tip and system has $s_0(\varepsilon) = 0$, while $|s_0(\varepsilon)| = 1$ in the absence of tunneling.

The generalization to 2D crystals modifies the projection operator $\hat{P}$. For a given dispersion relation $\xi(\mathbf{k})$ (measuring energies from the Fermi energy), the wave vectors $\mathbf{k}$ at a given energy ε are defined by $\xi(\mathbf{k}) = \varepsilon$. The angular distribution is governed by the Bloch function $u_{\mathbf{k}}(\boldsymbol{r}_0)$ at the position $\boldsymbol{r}_0$ of STM tip, so that the projection onto the single channel of the system is effected by the operator

$$\hat{P}\psi^{\text{in}}_{\mathbf{k}} = u_{\mathbf{k}}(\boldsymbol{r}_0) \sum_{\xi(\mathbf{k}')=\varepsilon} u^*_{\mathbf{k}'}(\boldsymbol{r}_0)\psi^{\text{in}}_{\mathbf{k}'} \equiv u_{\mathbf{k}}(\boldsymbol{r}_0)\langle u^*_{\mathbf{k}'}(\boldsymbol{r}_0)\psi^{\text{in}}_{\mathbf{k}'}\rangle_\varepsilon \quad (2)$$

with a properly normalized $u_{\mathbf{k}}(\boldsymbol{r}_0)$. Here, $\langle\ldots\rangle_\varepsilon$ stands for averaging over the constant-energy contour.

For contacts between normal-metal tip and superconductor, we extend the scattering matrix to Nambu space, using $s^*(-\varepsilon)$ instead of $s(\varepsilon)$ for holes [28,29]. Below, we exploit the particle-hole symmetry to focus on positive energies $\varepsilon > 0$. We also neglect the energy dependence of $s(\varepsilon)$, assuming it to be featureless for energies of the order of the gap $|\Delta|$.

Andreev and normal reflection.—An electron tunneling into the 2D sample forms an expanding particle wave $\psi^{(1)}_{p\mathbf{k}}$ with amplitude t and directional profile determined by the Bloch function, $\psi^{(1)}_{p\mathbf{k}} = tu_{\mathbf{k}}(\boldsymbol{r}_0)$. The superconductor retroreflects the particle into a counterpropagating hole [30]; see Fig. 1 for a sketch. When the coherence length is larger than the Fermi wavelength, we can account for Andreev reflection within the eikonal approximation: the Andreev amplitude $\alpha(\mathbf{k}, \varepsilon)$ depends on the superconducting gap $\Delta(\mathbf{k})$ at the same wave vector $\mathbf{k}$ allowing us to use the result of Refs. [28,29] at each $\mathbf{k}$,

$$\alpha_{p,h}(z) = \exp\left(\pm i \arg z - i \arccos|z|\right), \qquad z(\mathbf{k}, \varepsilon) = \frac{\varepsilon}{\Delta(\mathbf{k})}. \quad (3)$$

Here, $+(-)$ corresponds to $p \to h$ ($h \to p$) conversion [31]. We restrict considerations to a spin-singlet or polarized spin-triplet superconductor, so $\Delta(\mathbf{k})$ is viewed as a scalar. The analytical continuation to $|z| > 1$ is determined by the requirement $|\alpha_{p,h}| \le 1$.

The gap anisotropy becomes imprinted in the retroreflected wave, $\psi_{h\mathbf{k}} = \alpha_p(\mathbf{k})\psi^{(1)}_{p\mathbf{k}}$. Only part of it, $\hat{P}\psi_{h\mathbf{k}}$, scatters off the tip, while the complement, $(\hat{I} - \hat{P})\psi_{h\mathbf{k}}$, is oblivious to its presence. Thus, the hole escapes into the tip with amplitude $t^*\langle u^*_{\mathbf{k}}(\boldsymbol{r}_0)\alpha_p(\mathbf{k})\psi^{(1)}_{p\mathbf{k}}\rangle_\varepsilon$. The part of the hole wave $\psi_{h\mathbf{k}}$, which remains within the 2D material, takes the form $\psi^{(1)}_{h\mathbf{k}} = [(\hat{I} - \hat{P}) + s_0^*\hat{P}]\psi_{h\mathbf{k}}$, i.e.,

$$\psi^{(1)}_{h\mathbf{k}} = [\hat{I} - (1 - s_0^*)\hat{P}]\alpha_p(\mathbf{k})\psi^{(1)}_{p\mathbf{k}}, \qquad \psi^{(1)}_{p\mathbf{k}} = tu_{\mathbf{k}}(\boldsymbol{r}_0). \quad (4)$$

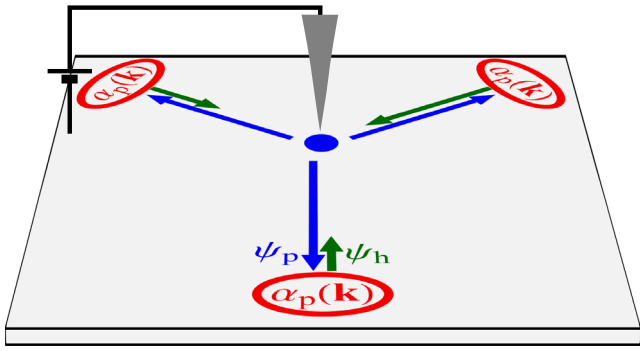

FIG. 1. Electron transport in a setup where an STM tip is placed over a high-symmetry point of a 2D superconductor. Symmetric blue arrows: the particle wave spreading from the tip carries the symmetry of crystalline lattice. Asymmetric green arrows: the Andreev-reflected hole wave [Eq. (4)] carries information about the superconducting gap symmetry, which may differ from the crystalline one.

Retroreflection of the hole wave reconverts it into a particle wave, $\alpha_h(\mathbf{k})\psi^{(1)}_{h\mathbf{k}}$. Similar to the hole, the particle splits between the tip and the 2D material with amplitudes $t\langle u^*_{\mathbf{k}}(\boldsymbol{r}_0)\alpha_h(\mathbf{k})\psi^{(1)}_{h\mathbf{k}}\rangle_\varepsilon$, and

$$\psi^{(2)}_{p\mathbf{k}} = [\hat{I} - (1 - s_0)\hat{P}]\alpha_h(\mathbf{k})\psi^{(1)}_{h\mathbf{k}}, \quad (5)$$

respectively. Then the process repeats: $\psi^{(2)}_{p\mathbf{k}}$ is retroreflected into a hole; the hole is partially absorbed into the tip with amplitude $t^*\langle u^*_{\mathbf{k}}(\boldsymbol{r}_0)\alpha_p(\mathbf{k})\psi^{(2)}_{p\mathbf{k}}\rangle_\varepsilon$ and partially scattered off it. Summing over cycles, we obtain the full Andreev-reflection (r_{ph} and r_{hp}) and normal-reflection (r_p and r_h) amplitudes. For example,

$$r_{ph} = |t|^2\left\langle u^*_{\mathbf{k}}(\boldsymbol{r}_0)\sum_{n=0}^{\infty}\hat{L}^n\alpha_p(\mathbf{k})u_{\mathbf{k}}(\boldsymbol{r}_0)\right\rangle_\varepsilon,$$
$$\hat{L} \equiv \alpha_p(\mathbf{k})[\hat{I} - (1 - s_0)\hat{P}]\alpha_h(\mathbf{k})[\hat{I} - (1 - s_0^*)\hat{P}]. \quad (6)$$

Symbolically performing the summation in Eq. (6) gives $r_{ph} = |t|^2\langle u^*_{\mathbf{k}}(\boldsymbol{r}_0)M(\mathbf{k})\rangle_\varepsilon$ with

$$M(\mathbf{k}) = (\hat{I} - \hat{L})^{-1}\alpha_p(\mathbf{k})u_{\mathbf{k}}(\boldsymbol{r}_0). \quad (7)$$

We recast Eq. (7) as the integral equation

$$(\hat{I} - \hat{L})M(\mathbf{k}) = \alpha_p(\mathbf{k})u_{\mathbf{k}}(\boldsymbol{r}_0). \quad (8)$$

Since the operator $\hat{L}$ has a separable kernel [32], we solve Eq. (8) by standard means [33] and express $M(\mathbf{k})$ in terms of three parameters:

$$a_{p,h} = \left\langle |u_{\mathbf{k}}(\boldsymbol{r}_0)|^2\frac{\alpha_{p,h}(\mathbf{k}, \varepsilon)}{1 - \alpha_p(\mathbf{k}, \varepsilon)\alpha_h(\mathbf{k}, \varepsilon)}\right\rangle_\varepsilon, \quad (9)$$

$$a_{ph} = \left\langle |u_{\mathbf{k}}(\boldsymbol{r}_0)|^2 \frac{\alpha_p(\mathbf{k},\varepsilon)\alpha_h(\mathbf{k},\varepsilon)}{1-\alpha_p(\mathbf{k},\varepsilon)\alpha_h(\mathbf{k},\varepsilon)} \right\rangle_{\varepsilon}. \quad (10)$$

Here, we restored the energy argument in $\alpha_{p,h}(\mathbf{k},\varepsilon)$. The averaging $\langle |u_{\mathbf{k}}(\boldsymbol{r}_0)|^2 \ldots \rangle_{\varepsilon}$ is defined by

$$\langle |u_{\mathbf{k}}(\boldsymbol{r}_0)|^2 \ldots \rangle_{\varepsilon} = \frac{\int d^2k \delta(\xi(\mathbf{k})-\varepsilon)|u_{\mathbf{k}}(\boldsymbol{r}_0)|^2 \ldots}{\int d^2k \delta(\xi(\mathbf{k})-\varepsilon)|u_{\mathbf{k}}(\boldsymbol{r}_0)|^2}. \quad (11)$$

Using the explicit form [33] of $M(\mathbf{k})$ in the expression for r_{ph}, we find the Andreev-refection amplitude

$$r_{ph} = \frac{|t|^2 a_p}{1+(2-s_0-s_0^*)a_{ph}+|1-s_0|^2(a_{ph}^2-a_p a_h)}. \quad (12)$$

Similarly, the normal-reflection amplitude is

$$r_p = s_0' + \frac{t^2[a_{ph}+(1-s_0^*)(a_{ph}^2-a_p a_h)]}{1+(2-s_0-s_0^*)a_{ph}+|1-s_0|^2(a_{ph}^2-a_p a_h)}. \quad (13)$$

The amplitudes r_{hp} and r_h are obtained from Eqs. (12) and (13) by replacing $a_p \leftrightarrow a_h$, $s_0 \leftrightarrow s_0^*$, and $t \leftrightarrow t^*$. Because of the unitarity of the scattering matrix Eq. (1), r_{ph} and $|r_p|$ depend only on a single matrix element s_0; its magnitude (but not phase) is fixed by $G_n/G_Q \equiv |t|^2 = 1-|s_0|^2$.

The Andreev- and normal-reflection amplitudes in Eqs. (12) and (13) depend on the energy ε of the incoming electron via Eqs. (9) and (10). The information on the gap structure $\Delta(\mathbf{k})$ and the crystal symmetry is encoded, respectively, in the $\mathbf{k}$-dependences of the retroreflection amplitudes Eq. (3) and the Bloch functions $u_{\mathbf{k}}(\boldsymbol{r}_0)$.

Differential conductance.—We can now express the differential conductance $G(V) = dI(V)/dV$ in terms of the amplitudes r_{ph} and r_p. For $V > 0$, one has [34]

$$G(V,\boldsymbol{r}_0) = G_Q[1-|r_p(eV,\boldsymbol{r}_0)|^2+|r_{ph}(eV,\boldsymbol{r}_0)|^2]. \quad (14)$$

The conductance for $V < 0$ follows by replacing $r_p(eV,\boldsymbol{r}_0) \to r_h(-eV,\boldsymbol{r}_0)$ and $r_{ph}(eV,\boldsymbol{r}_0) \to r_{hp}(-eV,\boldsymbol{r}_0)$.

Equations (9)–(14) provide a highly flexible framework for describing local tunneling spectroscopy of 2D superconductors and constitute the main advance of this Letter. They account for arbitrary superconducting gaps as well as the band structure, covering the entire crossover from weak to strong tunneling between tip and superconductor. While the weak-tunneling regime probes the local tunneling density of states, the strong-tunneling regime is dominated by Andreev processes, providing complementary information about the superconducting order parameter. Below, we illustrate the utility of our approach by focusing on several characteristic limits.

In the weak-tunneling limit $s_0 \to 1$, the differential conductance is governed by the tunneling density of states $\nu(eV)$ of the superconductor. Indeed, for $s_0 \to 1$, only the term $\propto a_{ph}$ in Eq. (13) contributes, so that Eq. (14) reduces to $G(V) = G_n\nu(eV)/\nu_n$ (with the tunneling density of states ν_n of the normal state). A fully gapped anisotropic superconductor with $\min\{|\Delta(\mathbf{k})|\} = \Delta_{\min}$ is signaled by zero conductance in the interval $|eV| < \Delta_{\min}$; see, e.g., Figs. 2(a),2(c)–2(e). In contrast, a nodal point in $\Delta(\mathbf{k})$ results in a V-shape profile $G(V) \sim G_n|eV|/\Delta$ at low biases; see Fig. 2(b); hereinafter, Δ is the characteristic value of $|\Delta(\mathbf{k})|$. Apart from this distinction, weak-tunneling data do not reveal the symmetry of the superconducting order parameter.

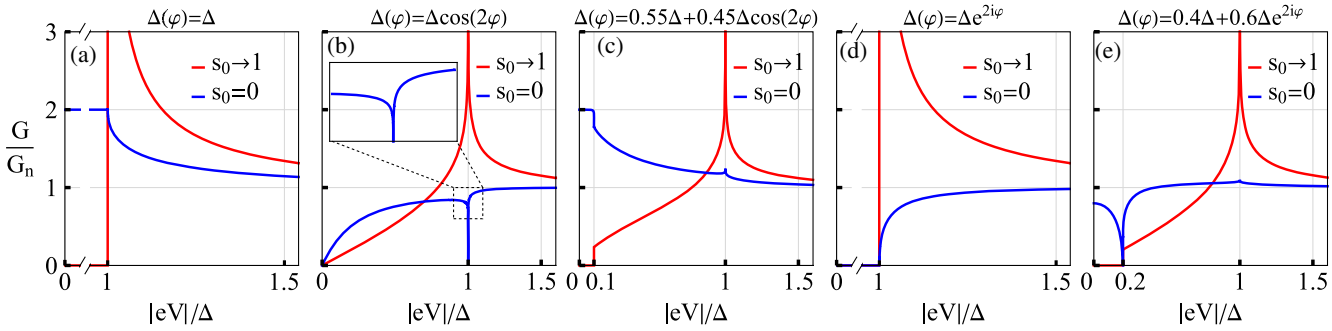

FIG. 2. Dependence of the normalized differential conductance G/G_n on bias V for weak ($s_0 \to 1$, red) and strong ($s_0 = 0$, blue) tunneling at a high-symmetry point. The conductance is evaluated with the help of Eqs. (9)–(14) for a 2D superconductor with a circular Fermi surface (parameterized by the angle φ) and gap $\Delta(\mathbf{k}) = \Delta(\varphi)$. (a) s-wave superconductor; (b) d-wave superconductor preserving time-reversal symmetry; $G(V)$ remains linear in the limit $V \to 0$ at any tunneling strength; the van Hove singularity at $s_0 \to 1$ is replaced by a Fano resonance (inset) at strong tunneling; (c) $s+d$ gap preserving time-reversal symmetry, but breaking the lattice point symmetry; parameters chosen to preserve the $G(0) = 2G_Q$, but significantly shrink the plateau $G(V) < 2G_Q$ at $V > 0$ compared to the case of s-wave superconductor [cf. (a)]; (d) $d+id$ gap preserving point-group symmetry, but breaking time-reversal symmetry; $G(V)$ remains zero below the gap at any s_0; (e) $s+d+id$ gap breaking point-group and time-reversal symmetries; a prominent Fano resonance develops at $eV = \min\{|\Delta(\varphi)|\}$ in the strong tunneling limit.

Complementary information on the gap structure is provided by Andreev reflections. This becomes most evident at zero bias $V = 0$, where the differential conductance is fully controlled by Andreev reflections, $|\alpha_{p,h}| = 1$ and hence $|r_{ph}|^2 + |r_p|^2 = 1$. In the corresponding limit $|\varepsilon| \to 0$, the Andreev amplitudes, Eq. (3), are $\alpha_p(\mathbf{k}) = -\alpha_h^*(\mathbf{k}) = -i\Delta(\mathbf{k})/|\Delta(\mathbf{k})|$. We can then evaluate Eqs. (14) and (12) for arbitrary junction conductance G_n and obtain

$$G(V = 0, \boldsymbol{r}_0) = 2G_Q |r_{ph}(\varepsilon = 0, \boldsymbol{r}_0)|^2,$$
$$r_{ph} = \frac{(2/i)(1 - |s_0|^2)\langle |u_{\mathbf{k}}(\boldsymbol{r}_0)|^2 \Delta(\mathbf{k})/|\Delta(\mathbf{k})|\rangle_0}{|1 + s_0|^2 + |1 - s_0|^2 |\langle |u_{\mathbf{k}}(\boldsymbol{r}_0)|^2 \Delta(\mathbf{k})/|\Delta(\mathbf{k})|\rangle_0|^2}. \tag{15}$$

This expression shows that the zero-bias conductance is sensitive to the interplay of the symmetries of the Bloch functions and the superconducting gap. Since the symmetry of the Bloch function varies with the tip position $\boldsymbol{r}_0$, it provides a powerful tool to extract the gap structure.

If $\boldsymbol{r}_0$ is invariant under the lattice point symmetry group, then $u_{\mathbf{k}}(\boldsymbol{r}_0)$ as a function of $\mathbf{k}$ belongs to an irreducible representation of the point group. Assuming that the only degeneracy of the Bloch states at the Fermi energy is associated with TRS, $u_{\mathbf{k}}(\boldsymbol{r}_0)$ belongs to a one-dimensional representation, i.e., $u_{\mathbf{k}}(\boldsymbol{r}_0)$ acquires only a phase factor and $|u_{\mathbf{k}}(\boldsymbol{r}_0)|^2$ is invariant under point-group operations. In contrast, there is no corresponding symmetry requirement when $\boldsymbol{r}_0$ is a generic point within the unit cell. Now consider the symmetry of $\Delta(\mathbf{k})/|\Delta(\mathbf{k})|$, entering into Eq. (15). First we note that $\sqrt{\xi^2(\mathbf{k}) + |\Delta(\mathbf{k})|^2}$ is an eigenvalue of the Bogoliubov–de-Gennes Hamiltonian. If $\Delta(\mathbf{k})$ does not break the lattice symmetry, then the eigenvalues of the Bogoliubov–de-Gennes Hamiltonian, as well as $\xi(\mathbf{k})$ are invariant under point-group transformations. Thus, $|\Delta(\mathbf{k})|$ belongs to the trivial representation [35], while $\Delta(\mathbf{k})/|\Delta(\mathbf{k})|$ together with $\Delta(\mathbf{k})$ belongs to some representation of the lattice point group. If that representation is trivial (as for s-wave superconductivity), then $\Delta(\mathbf{k})/|\Delta(\mathbf{k})|$ is independent of $\mathbf{k}$ and Eq. (15) reproduces the conventional result [34] $|r_{ph}| = (1 - |s_0|^2)/(1 + |s_0|^2)$, even if $\boldsymbol{r}_0$ is not a lattice symmetry point. With increasing tunneling strength, $G(V = 0)$ varies from $\sim G_n^2/G_Q$ at $s_0 \to 1$ to the saturation value $2G_Q$ at $s_0 = 0$.

If $\Delta(\mathbf{k})$ belongs to a nontrivial representation of the point group, then at a high-symmetry point the V shape of dI/dV with $G(V = 0, \boldsymbol{r}_0) = 0$ persists for any G_n; see Fig. 2(b), but $G(V = 0, \boldsymbol{r}_0)$ is finite at a generic $\boldsymbol{r}_0$. Lastly, if $\Delta(\mathbf{k})$ breaks the lattice symmetry, one expects a nonzero, position-dependent $G(V = 0, \boldsymbol{r}_0)$; depending on details, $G(0)$ may or may not reach the saturation value $2G_Q$, see also Figs. 2(c) and 2(e). One may understand these results pictorially; see Fig. 1. The total Andreev-reflection amplitude is a superposition of partial ones coming from the different directions $\mathbf{k}/|\mathbf{k}|$. Each partial amplitude carries a phase, governed by the gap an injected particle "sees" in the given direction. For a real-valued and symmetric nodal gap, the negative and positive contributions to the sum cancel each other. The presence of Bloch functions may lift the cancellation if their symmetry is different from that of the gap, or if the tunneling point is away from a high-symmetry point.

The conductance $G(V)$ depends strongly on the strength G_n of the tunneling contact; see Fig. 2. Focusing on the strong-tunneling limit of $s_0 = 0$ (i.e., $G_n = G_Q$), we can analytically extract the asymptotes of $G(V)$ for $V \to 0$ and $V \to \Delta$ [33].

We start with the $V \to 0$ asymptote. For a real-valued gap without nodal points (TRS is preserved, but spatial symmetry may be broken), we find $G(V) = 2G_Q[1 - \gamma_R(eV/\Delta)^4]$ to leading nontrivial order in eV/Δ. The coefficient $\gamma_R > 0$ depends on details of the gap structure as well as $\boldsymbol{r}_0$. For isotropic gaps, $\gamma_R = 0$ at any $\boldsymbol{r}_0$ and Eq. (14) is identical to known results in a one-dimensional geometry [34]. A real-valued gap with nodal points leads to $G(V) = G(0) + G_Q\gamma_V|eV|/\Delta$ with the sign of the coefficient γ_V depending on details of the gap and the tip position; for gaps respecting the lattice symmetry and $\boldsymbol{r}_0$ located at a symmetry point, $G(0) = 0$ and $\gamma_V > 0$, see Fig. 2(b). If the gap is complex valued and nodeless (broken TRS), but does not break the point-group symmetry (as in a $d_{x^2-y^2} + id_{xy}$ superconductor), we find $G(V) = 0$ in the entire interval $|eV| < \min\{\Delta(\mathbf{k})\}$ for tunneling at a symmetry point; see Fig. 2(d). Away from symmetry points, $G(V) = G(0) - G_Q\gamma_C|eV/\Delta|^2$ with model-dependent values of $G(0)$ and γ_C. If the point-group symmetry is broken in addition to TRS (as in noncollinear $A_2 + E_1 + iE_2$ states [36]), then $G(V) = G(0) - G_Q\gamma_C|eV/\Delta|^2$ with $G(0) < 2G_Q$ regardless of tip position; see Fig. 2(e). The coefficients γ_C in the last two asymptotes depend on the specific gap structure.

Extrema Δ_{extr} in $|\Delta(\mathbf{k})|$ lead to van Hove singularities in the tunneling density of states, which appear as "coherence peaks" $\propto \ln(\Delta_{\text{extr}}/|\Delta_{\text{extr}} - eV|)$ in the tunneling conductance at $G_n \ll G_Q$. At stronger tunneling, the peaks turn into singular minima of the form $A + B\ln^{-1}(\Delta_{\text{extr}}/|\Delta_{\text{extr}} - eV|)$ analogous to Fano resonances [Fig. 2(b)]. This structure becomes most prominent at full transmission ($s_0 = 0$), where $G(V)$ may vanish at the singularity; see, e.g., Figs. 2(b) and 2(e) [33].

Discussion and summary.—Our theory summarized in Eqs. (9)–(14) describes the differential conductance $G(V)$ in an STS setting for a 2D superconductor at arbitrary junction transmission as well as arbitrary symmetries of the order parameter and Bloch functions. The zero-bias results are expressed, in an intuitive way, by Eq. (15). We used the theory to perform a symmetry analysis of the conductance

and make specific predictions for tunneling both at and away from high-symmetry points of the lattice; see Fig. 2 and Table S1 [33] for further details.

Moiré materials such as TBG have a Fermi wavelength that is much larger than that of the metallic tip. Thus the single-channel-contact approximation is adequate unless the normal conductance G_n exceeds G_Q, indicating a substantial increase in a contact area. As long as the contact preserves its single-channel nature, the observation of a zero-bias conductance maximum at strong tunneling along with a prominent V-shaped conductance at weak tunneling, as reported in [12], is incompatible with a nodal gap respecting the lattice point symmetry. Indeed, in the latter case the low-bias behavior of $G(V)$ is linear at any tunneling strength; see, e.g., Fig. 2(b). The experimental data [12] for filling factors between -2 and -3 may be consistent with a strongly anisotropic gap with a small Δ_{min}, as exemplified in Fig. 2(c). However, while the superconducting gap symmetry of TBG is unknown, the required fine-tuning (e.g., between the strengths of s- and d-wave orders) would hardly persist over the entire filling-factor range [37]. A possible resolution [38] of this conundrum is provided by the data in Fig. S6 of Ref. [12]. There, the differential conductance is V-shaped as long as $G(V)$ remains below the maximal single-channel conductance $2G_Q$ for Andreev reflection. The V-shaped traces evolve into a zero-bias maximum only upon further increasing the junction conductance, where the tip may have developed a contact area of the order of the Moiré period and thus created a multichannel junction [38].

The differential conductance $G(V)$ in the STM setting was also recently obtained numerically in Ref. [39], using the tunneling Hamiltonian approach. For d- or p-wave superconductivity of TBG, the V-shaped dependence and the absence of a zero-bias peak persist for all tunneling strengths t_0. Our theory, applied under the same conditions, is consistent with the conclusions of Ref. [39], but also more nuanced. First, including the Bloch functions accounts for the dependence of $G(V)$ on the point of tunneling. In particular, $G(V=0)$ may be nonzero, even if the gap does not break the lattice symmetry. Second, our fully analytical solution based on scattering theory overcomes limitations of the tunneling Hamiltonian. At partial transmission, $G(V)$ depends not only on $t_0=\sqrt{1-|s_0|^2}$, but also on the *phase* of the scattering amplitude s_0. Accounting for the phase is important even at the qualitative level, affecting, e.g., the $V\to -V$ symmetry of $G(V)$ [33]. Our analytical solution also exposes the low-bias behavior of $G(V)$ and the emergence of a Fano resonance at stronger tunneling; see Fig. 2(b).

While we made several simplifying assumptions, our method applies more generally and allows for various extensions. For example, we assumed that, in the absence of tunneling, the tip does not create a scattering potential within the 2D material, i.e., $s_0(\varepsilon)=1$. Such a potential is readily incorporated through a scattering phase in s_0, leading to subgap resonances. Thus, our work provides a flexible and powerful framework to analyze future STM experiments aimed at revealing and analyzing the structure of the superconducting gap in TBG and other novel 2D superconductors.

This work was motivated by a discussion with Ali Yazdani at the Aspen Center for Physics supported by NSF Grant No. PHY-1607611. We are grateful to Piet Brouwer, Katharina Franke, and Vlad Kurilovich for illuminating remarks, and T. Senthil and Ali Yazdani for helpful comments. This work is supported by NSF Grant No. DMR-2002275 (L. I. G.), Deutsche Forschungsgemeinschaft through CRC 183 (Mercator fellowship, L. I. G.; project C02, F. v. O.) and a joint ANR-DFG project (TWISTGRAPH, F. v. O.). P. O. S. acknowledges support through the Yale Prize Postdoctoral Fellowship in Condensed Matter Theory.

*Corresponding author.
pavlo.sukhachov@yale.edu

[1] V. Mineev and K. Samokhin, *Introduction to Unconventional Superconductivity* (Taylor & Francis, Abingdon-on-Thames, 1999).
[2] J. G. Bednorz and K. A. Müller, Possible high T_c superconductivity in the Ba-La-Cu-O system, Z. Phys. B Condens. Matter **64**, 189 (1986).
[3] H. Maeda, Y. Tanaka, M. Fukutomi, and T. Asano, A new high-T_c oxide superconductor without a rare earth element, Jpn. J. Appl. Phys. **27**, L209 (1988).
[4] J. M. B. Lopes dos Santos, N. M. R. Peres, and A. H. Castro Neto, Graphene Bilayer with a Twist: Electronic Structure, Phys. Rev. Lett. **99**, 256802 (2007).
[5] E. Suárez Morell, J. D. Correa, P. Vargas, M. Pacheco, and Z. Barticevic, Flat bands in slightly twisted bilayer graphene: Tight-binding calculations, Phys. Rev. B **82**, 121407(R) (2010).
[6] R. Bistritzer and A. H. MacDonald, Moire bands in twisted double-layer graphene, Proc. Natl. Acad. Sci. U.S.A. **108**, 12233 (2010).
[7] Y. Cao, V. Fatemi, S. Fang, K. Watanabe, T. Taniguchi, E. Kaxiras, and P. Jarillo-Herrero, Unconventional superconductivity in magic-angle graphene superlattices, Nature (London) **556**, 43 (2018).
[8] M. Yankowitz, S. Chen, H. Polshyn, K. Watanabe, T. Taniguchi, D. Graf, A. F. Young, and C. R. Dean, Tuning superconductivity in twisted bilayer graphene, Science **363**, 1059 (2018).
[9] X. Lu, P. Stepanov, W. Yang, M. Xie, M. A. Aamir, I. Das, C. Urgell, K. Watanabe, T. Taniguchi, G. Zhang, A. Bachtold, A. H. MacDonald, and D. K. Efetov, Superconductors, orbital magnets, and correlated states in magic angle bilayer graphene, Nature (London) **574**, 653 (2019).
[10] Y. Cao, D. Rodan-Legrain, J. M. Park, F. N. Yuan, K. Watanabe, T. Taniguchi, R. M. Fernandes, L. Fu, and P. Jarillo-Herrero, Nematicity and competing orders in superconducting magic-angle graphene, Science **372**, 264 (2021).

[11] E. Y. Andrei and A. H. MacDonald, Graphene bilayers with a twist, Nat. Mater. **19**, 1265 (2020).

[12] M. Oh, K. P. Nuckolls, D. Wong, R. L. Lee, X. Liu, K. Watanabe, T. Taniguchi, and A. Yazdani, Evidence for unconventional superconductivity in twisted bilayer graphene, Nature (London) **600**, 240 (2021).

[13] H. Kim, Y. Choi, C. Lewandowski, A. Thomson, Y. Zhang, R. Polski, K. Watanabe, T. Taniguchi, J. Alicea, and S. Nadj-Perge, Spectroscopic signatures of strong correlations and unconventional superconductivity in twisted trilayer graphene, arXiv:2109.12127.

[14] O. Can, T. Tummuru, R. P. Day, I. Elfimov, A. Damascelli, and M. Franz, High-temperature topological superconductivity in twisted double layer copper oxides, Nat. Phys. **17**, 519 (2021).

[15] P. A. Volkov, J. H. Wilson, K. P. Lucht, and J. H. Pixley, Magic angles and current-induced topology in twisted nodal superconductors, Phys. Rev. B **107**, 174506 (2023).

[16] P. A. Volkov, S. Y. F. Zhao, N. Poccia, X. Cui, P. Kim, and J. H. Pixley, Josephson effects in twisted nodal superconductors, arXiv:2108.13456.

[17] P. A. Volkov, J. H. Wilson, K. Lucht, J. H. Pixley, Current- and Field-Induced Topology in Twisted Nodal Superconductors, Phys. Rev. Lett. **130**, 186001 (2023).

[18] S. Y. F. Zhao, N. Poccia, X. Cui, P. A. Volkov, H. Yoo, R. Engelke, Y. Ronen, R. Zhong, G. Gu, S. Plugge, T. Tummuru, M. Franz, J. H. Pixley, and P. Kim, Emergent interfacial superconductivity between twisted cuprate superconductors, arXiv:2108.13455.

[19] A. Damascelli, Z. Hussain, and Z.-X. Shen, Angle-resolved photoemission studies of the cuprate superconductors, Rev. Mod. Phys. **75**, 473 (2003).

[20] J. E. Hoffman, K. McElroy, D.-H. Lee, K. M. Lang, H. Eisaki, S. Uchida, and J. C. Davis, Imaging quasiparticle interference in $Bi_2Sr_2CaCu_2O_{8+\delta}$, Science **297**, 1148 (2002).

[21] K. McElroy, R. W. Simmonds, J. E. Hoffman, D.-H. Lee, J. Orenstein, H. Eisaki, S. Uchida, and J. C. Davis, Relating atomic-scale electronic phenomena to wave-like quasiparticle states in superconducting $Bi_2Sr_2CaCu_2O_{8+\delta}$, Nature (London) **422**, 592 (2003).

[22] Andreev reflection across a spatially extended (rather than local) junction of a *d*-wave superconductor with a normal metal was considered in Refs. [23–25].

[23] C. Bruder, Andreev scattering in anisotropic superconductors, Phys. Rev. B **41**, 4017 (1990).

[24] Y. Tanaka and S. Kashiwaya, Theory of Tunneling Spectroscopy of d-Wave Superconductors, Phys. Rev. Lett. **74**, 3451 (1995).

[25] S. Kashiwaya and Y. Tanaka, Tunnelling effects on surface bound states in unconventional superconductors, Rep. Prog. Phys. **63**, 1641 (2000).

[26] M. Ruby, F. Pientka, Y. Peng, F. von Oppen, B. W. Heinrich, and K. J. Franke, Tunneling Processes into Localized Subgap States in Superconductors, Phys. Rev. Lett. **115**, 087001 (2015).

[27] Microscopically, $|t(\varepsilon)|^2$ depends on the distance between the tip and the 2D material and the local density of states at the point of tunneling $\boldsymbol{r}_0$.

[28] C. W. J. Beenakker, Quantum transport in semiconductor-superconductor microjunctions, Phys. Rev. B **46**, 12841 (1992).

[29] Y. Nazarov and Y. Blanter, *Quantum Transport: Introduction to Nanoscience* (Cambridge University Press, Cambridge, 2009).

[30] A. F. Andreev, The thermal conductivity of the intermediate state in superconductors, J. Exp. Theor. Phys. **19**, 1228 (1964), http://jetp.ras.ru/cgi-bin/e/index/e/19/5/p1228?a=list.

[31] We will suppress the argument ε of $\alpha_{p,h}$ in the intermediate equations.

[32] P. Morse and H. Feshbach, *Methods of Theoretical Physics* (McGraw-Hill, New York, 1953).

[33] See Supplemental Material at http://link.aps.org/supplemental/10.1103/PhysRevLett.130.216002 for details of the scattering matrix approach, the explicit expressions for the conductance, and the additional numerical results.

[34] G. E. Blonder, M. Tinkham, and T. M. Klapwijk, Transition from metallic to tunneling regimes in superconducting microconstrictions: Excess current, charge imbalance, and supercurrent conversion, Phys. Rev. B **25**, 4515 (1982).

[35] M. Geier, P. W. Brouwer, and L. Trifunovic, Symmetry-based indicators for topological Bogoliubov–de Gennes Hamiltonians, Phys. Rev. B **101**, 245128 (2020).

[36] D. V. Chichinadze, L. Classen, and A. V. Chubukov, Nematic superconductivity in twisted bilayer graphene, Phys. Rev. B **101**, 224513 (2020).

[37] T. Senthil (private communication).

[38] A. Yazdani (private communication).

[39] E. Lake, A. S. Patri, and T. Senthil, Pairing symmetry of twisted bilayer graphene: A phenomenological synthesis, Phys. Rev. B **106**, 104506 (2022).